

SELF-ASSEMBLY OF SHALLOW MAGNETIC SPOTS THROUGH STRONGLY STRATIFIED TURBULENCE

AXEL BRANDENBURG^{1,2}, NATHAN KLEORIN^{1,3,4}, AND IGOR ROGACHEVSKII^{1,3,4}

¹ Nordita, Royal Institute of Technology and Stockholm University, Roslagstullsbacken 23, SE-10691 Stockholm, Sweden

² Department of Astronomy, AlbaNova University Center, Stockholm University, SE-10691 Stockholm, Sweden

³ Department of Mechanical Engineering, Ben-Gurion University of the Negev, POB 653, Beer-Sheva 84105, Israel

⁴ Department of Radio Physics, N. I. Lobachevsky State University of Nizhny Novgorod, Russia

Received 2013 June 20; accepted 2013 September 19; published 2013 October 3

ABSTRACT

Recent studies have demonstrated that in fully developed turbulence, the effective magnetic pressure of a large-scale field (non-turbulent plus turbulent contributions) can become negative. In the presence of strongly stratified turbulence, this was shown to lead to a large-scale instability that produces spontaneous magnetic flux concentrations. Furthermore, using a horizontal magnetic field, elongated flux concentrations with a strength of a few percent of the equipartition value were found. Here we show that a uniform *vertical* magnetic field leads to circular magnetic spots of equipartition field strengths. This could represent a minimalistic model of sunspot formation and highlights the importance of two critical ingredients: turbulence and strong stratification. Radiation, ionization, and supergranulation may be important for realistic simulations, but are not critical at the level of a minimalistic model of magnetic spot formation.

Key words: magnetohydrodynamics (MHD) – starspots – sunspots – turbulence

Online-only material: color figures

1. INTRODUCTION

Over the last 30 yr, there has been a growing consensus that sunspots are the surface interceptions of long thin flux tubes that are anchored deep near the bottom of the convection zone (Parker 1975; Spiegel & Weiss 1980; D’Silva & Choudhuri 1993). By contrast, direct numerical simulations (DNS) of global convectively driven dynamos produce a magnetic field that is distributed throughout the convection zone (Brown et al. 2011), either with a maximum at the bottom of the convection zone (Racine et al. 2011) or at mid depths (Käpylä et al. 2012a). Furthermore, while DNS have been able to demonstrate the ascent of thin flux tubes within a stratified layer (Fan 2001), convection simulations such as those of Guerrero & Käpylä (2011) have not produced evidence that sufficiently strong tubes are a natural result of a dynamo. On the contrary, once simulations develop large-scale dynamo action, they produce a more diffusive large-scale field with a filling factor close to unity (Käpylä et al. 2008), which suggests that the large-scale field is more densely packed and not in the form of thin tubes. These types of arguments have led to the proposal that the solar dynamo may be a distributed one and that sunspots and active regions may be a shallow phenomenon (Brandenburg 2005).

The alternative scenario of a shallow origin of active regions and sunspots faces difficulties too. Simulations of Rempel (2011) have shown that a realistic, sunspot-like appearance of the magnetic field can be obtained when the field is kept fixed at the bottom of the domain. Related simulations have also been done for bipolar spots (Cheung et al. 2010). Both studies emphasize the importance of radiative transfer. While this is also true for the simulations of Stein & Nordlund (2012), they do demonstrate that keeping the flux tubes fixed in space might not be needed if the computational domain is big enough and new horizontal field of 1 kG is continuously supplied from the bottom of their domain. They interpret their findings in terms of magnetic flux being swept down and kept in place at

greater depth by the strong converging flows associated with the supergranulation. Yet another radiative magnetohydrodynamics simulation with realistic physics is that of Kitiashvili et al. (2010), who also find spontaneous flux concentrations as a result of strongly converging flows, even though their domain is more shallow and without supergranulation. This work might also be related to that of Tao et al. (1998), who showed that magneto-convection tends to segregate into magnetized and unmagnetized regions.

The purpose of the present paper is to emphasize that the spontaneous assembly of magnetic flux can be caused by purely hydromagnetic effects without involving convection, supergranulation, radiative transport, or even energy flux. Our proposal is based on recent numerical evidence that the so-called negative effective magnetic pressure instability (NEMPI), which was originally discovered in analytical studies by Kleorin et al. (1989, 1990), does really work (Brandenburg et al. 2011; Kemel et al. 2012a, 2012b, 2013). However, a serious problem with this approach was that in the presence of an imposed horizontal magnetic field, the strongest flux concentrations are typically just some 10% of the equipartition value. We now show that this restriction is alleviated when there is a small vertical net flux through the domain. In that case the magnetic field arranges itself in the form of a spot-like assembly that is fully confined by the turbulent flow itself, without the need for keeping it in place by artificial means.

The underlying mechanism of NEMPI is based on the suppression of turbulent pressure and has been studied analytically (Kleorin & Rogachevskii 1994; Rogachevskii & Kleorin 2007) and numerically (Brandenburg et al. 2012; Losada et al. 2012, 2013a; Jabbari et al. 2013), using mean-field simulations (MFS) and DNS. It can be understood as a negative contribution of turbulence to the effective mean magnetic pressure (the sum of non-turbulent and turbulent contributions). At large Reynolds numbers this turbulent contribution becomes large and NEMPI can be excited. The presence of strong density stratification (small density scale height, H_ρ) is crucial, because it leads to a

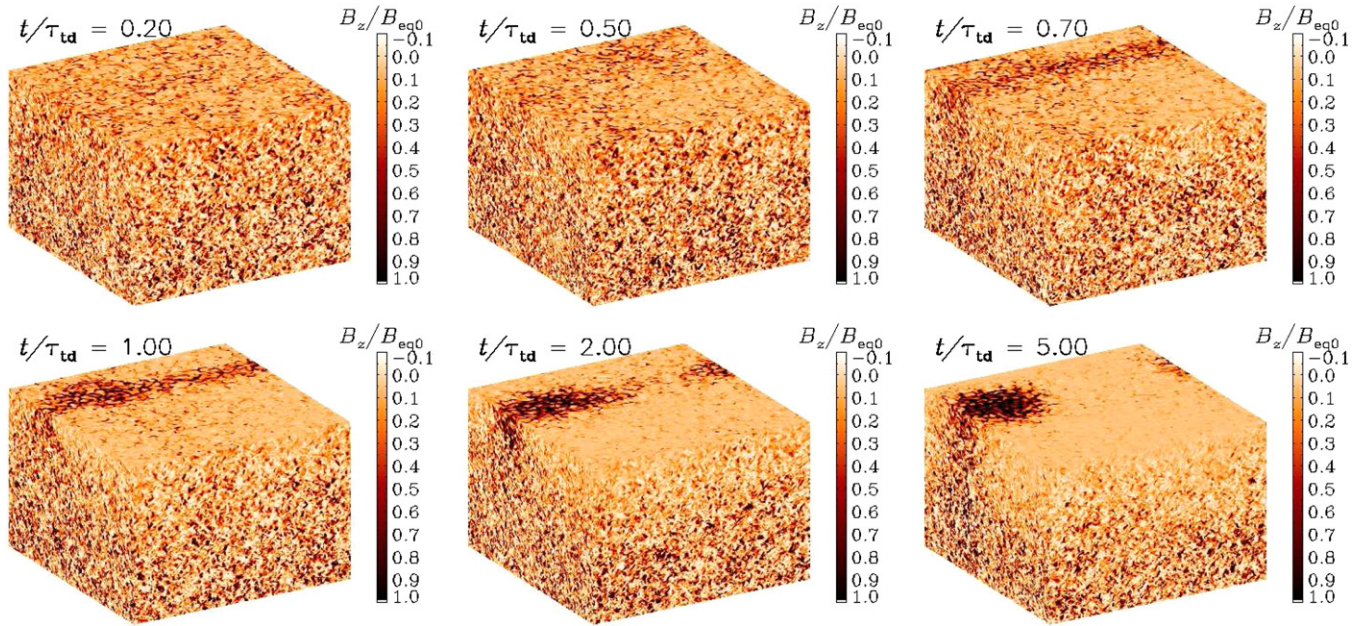


Figure 1. Evolution from a uniform initial state toward a circular spot for $B_{z0}/B_{eq0} = 0.02$. Here, B_z/B_{eq0} is shown on the periphery of the domain. Dark shades correspond to strong vertical fields. Time is in units of τ_{td} . An animation is available on http://youtu.be/Um_7Hs_1RzA. (A color version of this figure is available in the online journal.)

negative magnetic buoyancy force. (A local increase of the magnetic field causes a decrease of the negative effective magnetic pressure, which is compensated for by enhanced gas pressure, leading to enhanced gas density, so the gas is heavier than its surroundings and sinks.) This results in a positive feedback loop: downflow compresses the field, the effective magnetic pressure becomes more negative, gas pressure increases, so the density increases, and the downflow accelerates; see Equations (4)–(9) of Kemel et al. (2013) for a phenomenological approach. However, for magnetic fields close to equipartition, the effective magnetic pressure becomes positive again, so the instability saturates. Significant scale separation between the forcing scale and the size of the domain (about 15–30) is important, because smaller turbulent eddies imply smaller turbulent diffusion; see Figure 17 of Brandenburg et al. (2012).

2. DETAILS OF THE MODEL

Our goal is to present a minimalistic model capable of producing a magnetic spot. Within the framework of NEMPI, all that is needed is turbulence, large enough scale separation, and strong stratification. Our basic setup was described in Brandenburg et al. (2011, 2012), where non-helically driven turbulence was simulated in an isothermally stratified domain. In that case, H_ρ is constant, so the effects of strong stratification are distributed over all heights. The forcing consists of random plane waves with constant amplitude, so the rms velocity of the turbulence, u_{rms} , is independent of z . As shown by Kemel et al. (2012b), the theoretically expected maximum growth rate of NEMPI, $\lambda_0 \approx \beta_* u_{rms}/H_\rho$, is then the same for magnetic fields at different heights, although the depth where NEMPI is excited, increases with increasing field strength. Here, β_* is a non-dimensional parameter that was found to be around 0.3 for magnetic Reynolds numbers in the range $1 \lesssim \text{Re}_M \lesssim 60$, and 0.2 is for larger Re_M , when small-scale dynamo action is possible (Brandenburg et al. 2012). Furthermore, in addition to isothermal stratification, the equation of state is assumed isothermal, so the stabilizing effects from

Brunt-Väisälä oscillations are absent (see Käpylä et al. 2012b, where this has been relaxed in some of their MFS). The scale separation ratio is taken to be 30, i.e., there are on average 30 turbulent cells across the domain; see Losada et al. (2013a) and Brandenburg et al. (2013), where magnetic energy spectra are shown.

The simulations are performed with the PENCIL CODE,⁵ which uses sixth-order explicit finite differences in space and a third-order accurate time stepping method. The magnetic field \mathbf{B} is expressed in terms of the magnetic vector potential A such that $\mathbf{B} = \mathbf{B}_0 + \nabla \times A$ is divergence-free and $\mathbf{B}_0 = (0, 0, B_0)$ is the imposed vertical field. We use a numerical resolution of 256^3 mesh points in a Cartesian domain (x, y, z) of size L^3 such that $-L/2 < x, y, z < L/2$. Our boundary conditions are periodic in the horizontal directions (so vertical magnetic flux is conserved), and stress free on the upper and lower boundaries where the field is assumed to be vertical, i.e., $B_x = B_y = 0$. Unless mentioned otherwise, the initial magnetic field is uniform ($A = 0$, so $\mathbf{B} = \mathbf{B}_0$) and our simulations are started from scratch.

Time is expressed in turbulent-diffusive times, $\tau_{td} = H_\rho^2/\eta_{t0}$, where $\eta_{t0} = u_{rms}/3k_f$ is the estimated turbulent magnetic diffusivity and k_f is the wavenumber of the energy-carrying eddies. Their turnover time is $\tau_{to} = 1/u_{rms}k_f = \tau/k_f H_\rho$, where $\tau = H_\rho/u_{rms}$ is the natural time scale in a stratified layer. Thus, $\tau_{td}/\tau = 3k_f H_\rho$ and $\tau_{td}/\tau_{to} = 3(k_f H_\rho)^2$. We use a setup that is similar to that of Kemel et al. (2012a), where $H_\rho = 1$ and $L = 2\pi$, so we have $L/H_\rho = 2\pi \approx 6$ scale heights across the domain. The magnetic Reynolds number based on the wavenumber k_f is $\text{Re}_M = u_{rms}/\eta k_f \approx 19$, with η being the microphysical magnetic diffusivity, while that based on the scale L is about 570. The magnetic Prandtl number is $1/2$ and the fluid Reynolds number is 38, but simulations at resolutions of up to 1024^3 and $\text{Re}_M = 95$ give similar results (Brandenburg et al. 2013). The magnetic field is normalized

⁵ <http://pencil-code.googlecode.com>

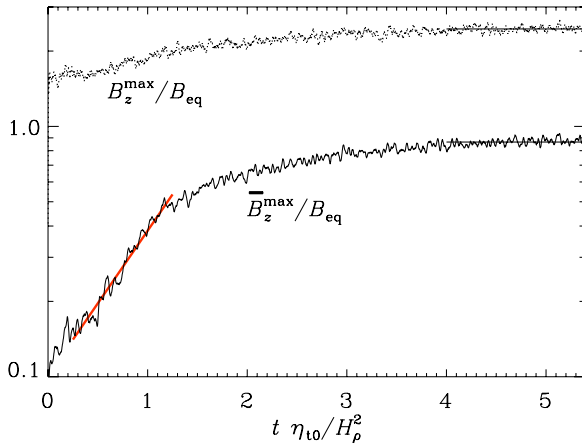


Figure 2. Growth of $\overline{B}_z^{\max}/B_{\text{eq}}(z)$ (solid) and $B_z^{\max}/B_{\text{eq}}(z)$ (dotted) at the top boundary. The straight red line corresponds to a growth rate of $1.3 \eta_{10}/H_\rho^2$. (A color version of this figure is available in the online journal.)

by the local equipartition field strength, $B_{\text{eq}}(z) = (\mu_0 \overline{\rho})^{1/2} u_{\text{rms}}$, where μ_0 is the vacuum permeability, $\overline{\rho}(z)$ is the horizontally averaged density, while for u_{rms} we take the root-mean-square based on a volume average, because the turbulent velocity is driven such that it does not show systematic height dependence. (Since B_0 is small, the global u_{rms} does not change noticeably during the simulation.) We also define $B_{\text{eq}0} = B_{\text{eq}}(z = 0)$ to specify the strength of the imposed vertical magnetic field, as well as $B_{\text{eq}}(x)$ and $\overline{B}_{\text{eq}}(x)$ to characterize the local horizontal variation of $(\mu_0 \rho u^2)^{1/2}$ through the magnetic spot. Overbars denote Fourier filtering, as explained below.

3. RESULTS

We have studied cases with different values of B_0 . We begin with $B_0/B_{\text{eq}0} = 0.02$ and show in Figure 1 the time evolution of the vertical magnetic field, B_z , on the periphery of the domain. Here, dark shades correspond to strong fields, so as to give an idea how the temperature might look like if we relaxed the isothermal assumption. Note in particular the gradual assembly of a magnetic spot from a uniform turbulent background. The

color table is clipped for field strengths above the equipartition value, while the field peaks at twice this value. The time required for the development a magnetic spot is 2–5 turbulent-diffusive times.

The growth of the large-scale field is compatible with an exponential one with a growth rate $\lambda \approx 1.3 \eta_{10}/H_\rho^2$; see Figure 2, where we show, at the top layer, the maximum field strength, B_z^{\max} , and the maximum value of the large-scale field, \overline{B}_z^{\max} , obtained by Fourier filtering to include only fields with horizontal wavenumbers below $k_f/6$. Our value of λ agrees with that of earlier studies of magnetic flux concentrations in DNS in the presence of a horizontal field and related MFS of NEMPI (Kemel et al. 2012a). However, our domain might not be large enough to include the horizontal wavenumber k_\perp of the fastest growing mode, which has $k_\perp H_\rho \approx 0.7$ (Brandenburg et al. 2013). On the other hand, once the instability saturates, the magnetic field in the direction of the imposed field gets more concentrated and is then fully confined in the domain. Between $t/\tau_{\text{id}} = 2$ and 5, it develops into a nearly circular spot, as might be expected from cylindrical symmetry arguments.

In Figure 3 we show horizontal and vertical cuts through the spot. In the horizontal cut, again, strong fields correspond to dark shades. The vertical cut is with a different color table where strong fields now correspond to light shades. It shows that the magnetic field (in units of the local equipartition field strength) decreases with depth, but that fluctuations of both signs (blue and yellow shades, respectively) become stronger. We also consider the field averaged azimuthally about the vertical axis of the tube. Field lines correspond to contours of $\overline{A}_\theta(\overline{\omega}, z)$, where $(\overline{\omega}, \theta, z)$ are cylindrical polar coordinates with $\overline{\omega}$ being the cylindrical radius, θ the azimuthal angle, and z is identical to the Cartesian vertical coordinate. This shows that the field in the tube fans out toward the bottom of the domain and that the spot is only loosely anchored.

To analyze the magnetic spot quantitatively, we show in Figure 4 horizontal and vertical cross-sections for the snapshot shown in Figure 3. It turns out that at some level $z = z_1$, the increase of $\overline{B}_z(x)$ at the position of the tube is matched by a corresponding decrease in $\overline{B}_{\text{eq}}(x)$; see Figure 4(a). We recall that $B_{\text{eq}}(x)$ was defined in Section 2 without averaging so as to see its local suppression at the position of the spot.

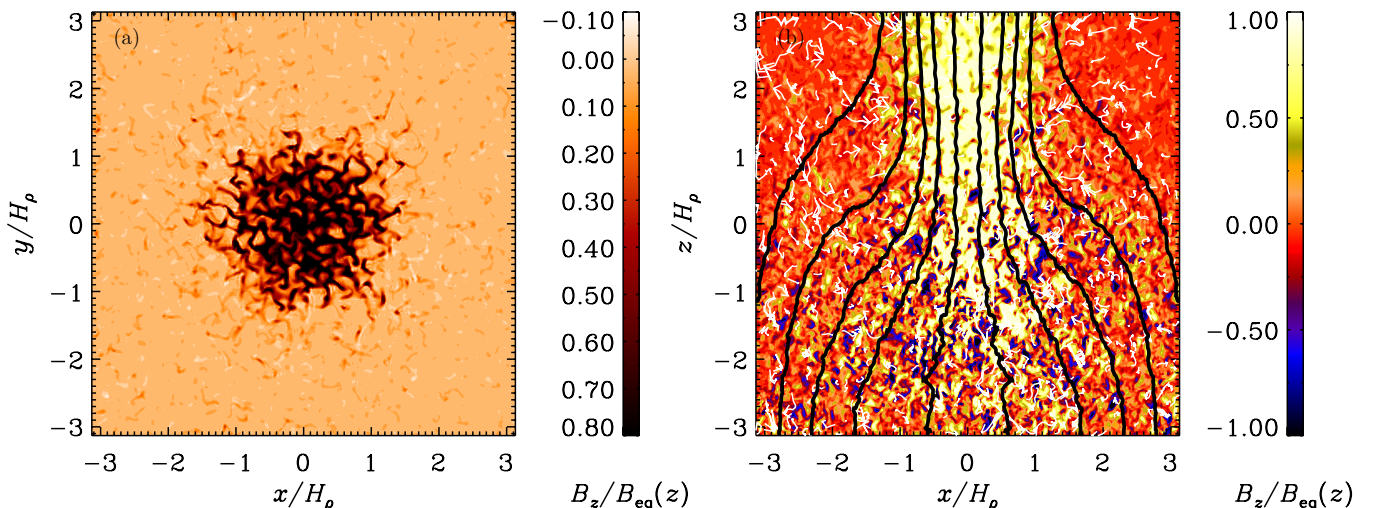


Figure 3. Cuts of $B_z/B_{\text{eq}}(z)$ in the xy plane at the top boundary ($z/H_\rho = \pi$) and the xz plane through the middle of the spot at $y = 0$. In the xz cut, we also show magnetic field lines and flow vectors obtained by numerically averaging in azimuth around the spot axis.

(A color version of this figure is available in the online journal.)

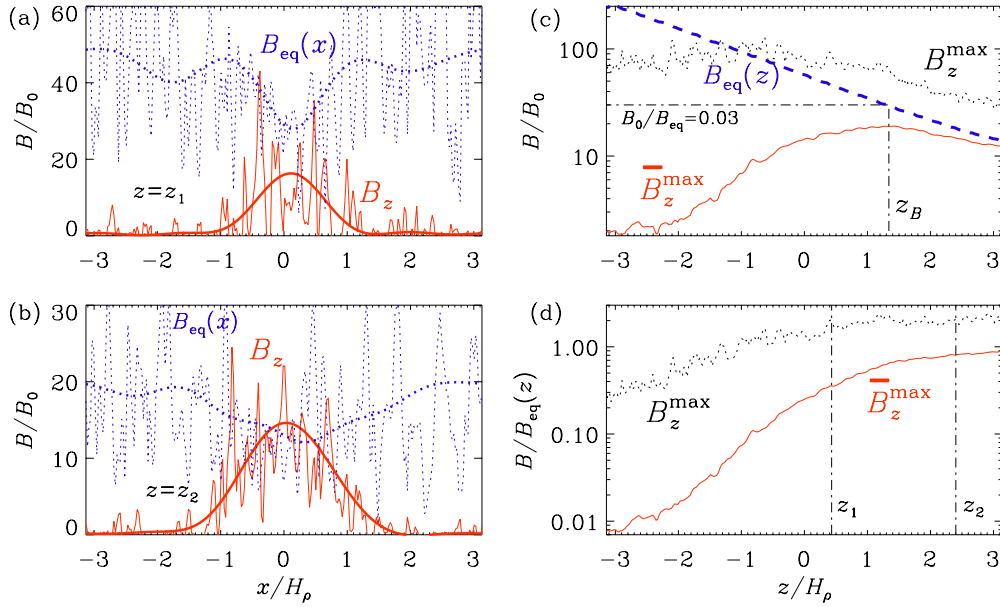


Figure 4. Horizontal cross-tube profiles of $B_{\text{eq}}(x)$ and B_z , where the smooth curves show, respectively, the spatial distribution of $\bar{B}_{\text{eq}}(x)$ and \bar{B}_z , normalized by B_0 , through $z = z_1 \equiv 0.4 H_\rho$ (a) and $z = z_2 \equiv 2.4 H_\rho$ (b), and vertical profiles of \bar{B}_z^{max} , B_z^{max} , and $B_{\text{eq}}(z)$ normalized by B_0 (c) and by $B_{\text{eq}}(z)$ (d) for the snapshot shown in Figure 1. Dash-dotted lines denote in (c) the height z_B where $B_0/B_{\text{eq}}(z_B) \approx 0.03$, and in (d) the positions z_1 and z_2 . (A color version of this figure is available in the online journal.)

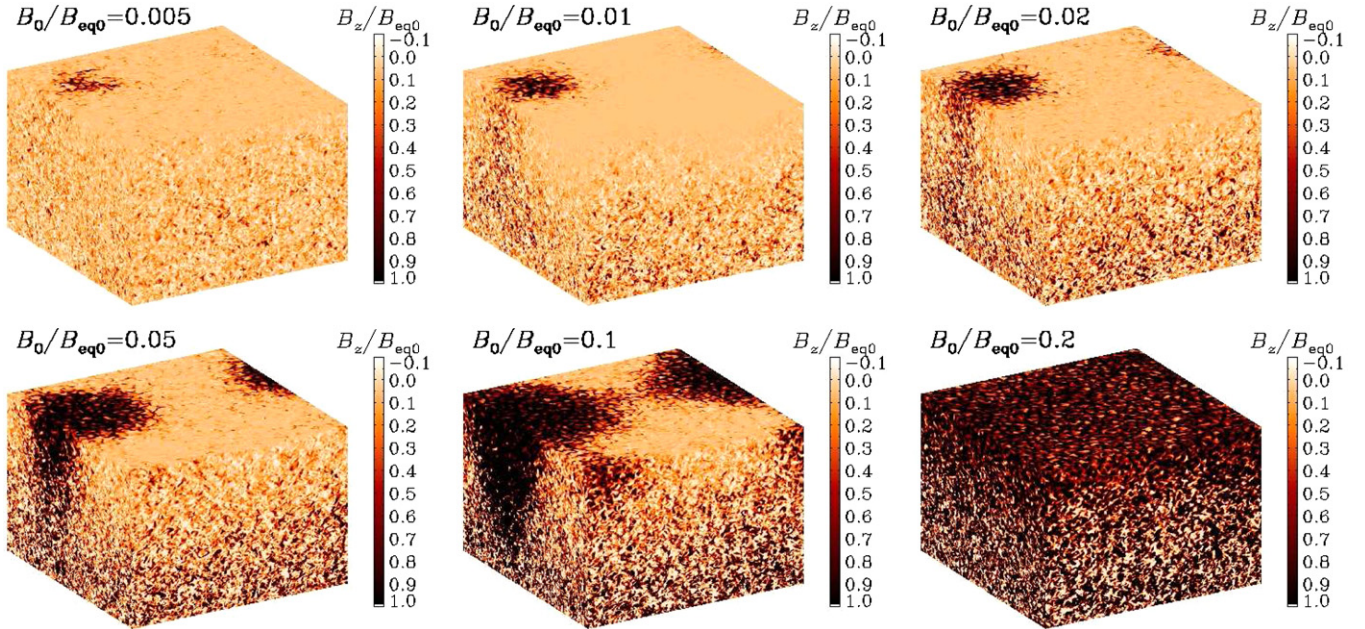


Figure 5. Magnetic field structure for $B_0/B_{\text{eq}0}$ ranging from 0.005 to 0.2 showing the gradual transition from a small spot to a fully covered surface. (A color version of this figure is available in the online journal.)

At higher levels, only a small portion of the turbulent kinetic energy is required to sustain the spot; see Figure 4(b) at $z = z_2$. As a function of height, $B_{\text{eq}}(z)$ decreases monotonously. Therefore, although the large-scale field representing the spot, $\bar{B}_z^{\text{max}}/B_0$, has a maximum at $z/H_\rho \approx 1$, as seen in Figure 4(c), the field in units of the equipartition field, $\bar{B}_z^{\text{max}}/B_{\text{eq}}(z)$, reaches a plateau in $1.5 \lesssim z/H_\rho \lesssim 3$; see Figure 4(d). This is compatible with results by Losada et al. (2013b) that for a vertical field the instability is strongest at a height z_B where $B_0/B_{\text{eq}}(z_B) \approx 0.03$. This is the case somewhere between z_1 and z_2 , where $B_{\text{eq}}(z)/B_0 \approx 30$ in Figure 4(c). Yet, in the nonlinear regime, near-equipartition field strengths are possible

in the upper part—both in DNS and the aforementioned MFS (Brandenburg et al. 2013). Such sustained flux concentrations might be assisted by slow inflows, as seen in the upper part of Figure 3(b).

Finally, in Figure 5 we compare simulations with different imposed field strengths with $B_0/B_{\text{eq}0}$ from 5×10^{-3} to 0.2. The third panel corresponds to the last one of Figure 1, which was also used as initial condition for the other runs. The spot becomes smaller for weaker fields, while for stronger fields the surface is eventually fully covered. Note, however, that in all cases the large-scale field is approximately of equipartition strength and roughly independent of the strength of the imposed fields. This

is interesting in view of the fact that photospheric magnetic fields of active stars are found to be of thermal equipartition strength such that the filling factor grows as the star becomes more active (Saar & Linsky 1985).

We emphasize that the magnetic field is not uniform across the spot, as is assumed in a monolithic sunspot model, but it is more reminiscent of the fibril sunspot model of Parker (1979). In our case, there can even be regions where the field has the opposite sign. This explains why in the last panel of Figure 5 the field reaches peak values above the equipartition value over the entire horizontal plane—without violating flux conservation, even though the large-scale field is only 20% of the equipartition value. The value of $u_{\text{rms}}/c_s \approx 0.094$ is slightly less than its original value of ≈ 0.12 .

4. CONCLUSIONS

The present work has demonstrated two important aspects in the production of magnetic flux concentrations: the presence of a vertical magnetic field favors the formation of circular structures and their field strengths can exceed the local equipartition value. The reason for such a strong effect in comparison with the case with a horizontal imposed field is the apparent absence of the so-called potato sack effect (cf. Brandenburg et al. 2011). We argue that this is a direct consequence of the negative effective magnetic pressure, making such horizontal magnetic structures heavier than their surroundings. The potato sack effect is a nonlinear mechanism responsible for a premature saturation of NEMPI with a horizontal field, because it removes horizontal magnetic flux structures from regions in which NEMPI is excited. For a vertical magnetic field, the heavier fluid moves downward along the field without affecting the flux tube, so that NEMPI is not stabilized by the potato sack effect. Instead, NEMPI saturates when $\overline{B}_z^{\text{max}}/B_{\text{eq}}(z) = O(1)$; see Figure 4(d).

Application to the Sun is premature, but tentatively we might estimate the time of spot formation in solar values by using $u_{\text{rms}} = 1 \text{ km s}^{-1}$ and $H_\rho = 300 \text{ km}$, so $\tau = H_\rho/u_{\text{rms}} \approx 5$ minutes. This, together with $k_f H_\rho \approx 2\pi\gamma/\alpha_{\text{mix}} \approx 6.5$ (Losada et al. 2013a), gives $\tau_{\text{td}} \approx 3 \times 6.5 \times \tau \approx 100$ minutes, and thus five turbulent-diffusive times correspond to 8 hr on a NEMPI length scale of $(2\pi/0.7) \times 300 \text{ km} \approx 3 \text{ Mm}$; see Section 2. Here, $\gamma = 5/3$ is the ratio of specific heats, $\alpha_{\text{mix}} = 1.6$ is the mixing length parameter, and $k_\perp H_\rho \approx 0.7$ has been used (Brandenburg et al. 2013). Conversely, at a depth where $H_\rho = 3 \text{ Mm}$, the length scale would be 30 Mm and $5\tau_{\text{td}} \approx 80 \text{ hr} \approx 3$ days. Furthermore, using $\rho = 10^{-5} \text{ g cm}^{-3}$, we have $B_{\text{eq}} \approx 1 \text{ kG}$, so our model with $\overline{B}_z^{\text{max}}/B_{\text{eq}}(z) \leq 1$ might fall short of explaining the 3 kG field strengths observed in sunspots.

Our estimates are based on a minimalistic model of sunspot formation. Nevertheless, these new findings of flux concentrations with vertical fields warrant further research in studying the origin of sunspots and active regions. Future developments include the addition of (1) a radiating surface to move the top boundary condition away from the upper boundary of the spot, (2) hydrogen ionization to allow for an extreme temperature jump that might enhance the local growth of NEMPI, (3) dynamo-generated instead of imposed fields to allow spots to come and go as the large-scale field evolves, and finally (4) convection instead of forced turbulence to have a natural scale of turbulence with changes in its strength in response to the magnetic field.

Studies involving radiation and ionization require the solution of an energy equation, which might be important for obtaining

larger field strengths. The simultaneous presence of NEMPI and dynamo instability has already been studied in global MFS (Jabbari et al. 2013) as well as in local DNS in Cartesian geometry (Losada et al. 2013a). The allowance for dynamo action is particularly important from a morphological point of view. It would give us a better idea about the appearance and disappearance of spots, the possibility of bipolar regions (Warnecke et al. 2013), and their inclination relative to the east–west direction, which is expected due to the combined presence of poloidal and toroidal fields in a dynamo. Again, radiation might be important to allow the field to develop more realistic inclinations about the vertical and thereby also the formation of a penumbra.

We thank the three anonymous reviewers for their detailed comments and suggestions that have greatly improved the paper. Computing resources provided by the Swedish National Allocations Committee at the Center for Parallel Computers at the Royal Institute of Technology in Stockholm and the High Performance Computing Center North in Umeå. This work was supported in part by the European Research Council under the AstroDyn Research Project No. 227952, by the Swedish Research Council under the project grants 621-2011-5076 and 2012-5797, by EU COST Action MP0806, by the European Research Council under the Atmospheric Research Project No. 227915, and by a grant from the Government of the Russian Federation under contract No. 11.G34.31.0048.

REFERENCES

- Brandenburg, A. 2005, *ApJ*, **625**, 539
- Brandenburg, A., Gressel, O., Jabbari, S., Kleeorin, N., & Rogachevskii, I. 2013, *A&A*, submitted (arXiv:1309.3547)
- Brandenburg, A., Kemel, K., Kleeorin, N., Mitra, D., & Rogachevskii, I. 2011, *ApJL*, **740**, L50
- Brandenburg, A., Kemel, K., Kleeorin, N., & Rogachevskii, I. 2012, *ApJ*, **749**, 179
- Brown, B. P., Miesch, M. S., Browning, M. K., Brun, A. S., & Toomre, J. 2011, *ApJ*, **731**, 69
- Cheung, M. C. M., Rempel, M., Title, A. M., & Schüssler, M. 2010, *ApJ*, **720**, 233
- D’Silva, S., & Choudhuri, A. R. 1993, *A&A*, **272**, 621
- Fan, Y. 2001, *ApJ*, **554**, L111
- Jabbari, S., Brandenburg, A., Kleeorin, N., Mitra, D., & Rogachevskii, I. 2013, *A&A*, **556**, A106
- Guerrero, G., & Käpylä, P. J. 2011, *A&A*, **533**, A40
- Käpylä, P. J., Brandenburg, A., Kleeorin, N., Mantere, M. J., & Rogachevskii, I. 2012b, *MNRAS*, **422**, 2465
- Käpylä, P. J., Korpi, M. J., & Brandenburg, A. 2008, *A&A*, **491**, 353
- Käpylä, P. J., Mantere, M. J., & Brandenburg, A. 2012a, *ApJL*, **755**, L22
- Kemel, K., Brandenburg, A., Kleeorin, N., Mitra, D., & Rogachevskii, I. 2012a, *SoPh*, **280**, 321
- Kemel, K., Brandenburg, A., Kleeorin, N., Mitra, D., & Rogachevskii, I. 2013, *SoPh*, **287**, 293
- Kemel, K., Brandenburg, A., Kleeorin, N., & Rogachevskii, I. 2012b, *AN*, **333**, 95
- Kitiashvili, I. N., Kosovichev, A. G., Wray, A. A., & Mansour, N. N. 2010, *ApJ*, **719**, 307
- Kleeorin, N., & Rogachevskii, I. 1994, *PhRvE*, **50**, 2716
- Kleeorin, N. I., Rogachevskii, I. V., & Ruzmaikin, A. A. 1989, *SvAL*, **15**, 274
- Kleeorin, N. I., Rogachevskii, I. V., & Ruzmaikin, A. A. 1990, *Sov. Phys. JETP*, **70**, 878
- Losada, I. R., Brandenburg, A., Kleeorin, N., Mitra, D., & Rogachevskii, I. 2012, *A&A*, **548**, A49
- Losada, I. R., Brandenburg, A., Kleeorin, N., & Rogachevskii, I. 2013a, *A&A*, **556**, A83
- Losada, I. R., Brandenburg, A., Kleeorin, N., & Rogachevskii, I. 2013b, *A&A*, submitted (arXiv:1307.4945)
- Parker, E. N. 1975, *ApJ*, **198**, 205

- Parker, E. N. 1979, [ApJ](#), **234**, 333
- Racine, É., Charbonneau, P., Ghizaru, M., Bouchat, A., & Smolarkiewicz, P. K. 2011, [ApJ](#), **735**, 46
- Rempel, M. 2011, [ApJ](#), **740**, 15
- Rogachevskii, I., & Kleeorin, N. 2007, [PhRvE](#), **76**, 056307
- Saar, S. H., & Linsky, J. L. 1985, [ApJ](#), **299**, L47
- Spiegel, E. A., & Weiss, N. O. 1980, [Natur](#), **287**, 616
- Stein, R. F., & Nordlund, Å. 2012, [ApJL](#), **753**, L13
- Tao, L., Weiss, N. O., Brownjohn, D. P., & Proctor, M. R. E. 1998, [ApJ](#), **496**, L39
- Warnecke, J., Losada, I. R., Brandenburg, A., Kleeorin, N., & Rogachevskii, I. 2013, [ApJ](#), submitted (arXiv:1308.1080)